Please cite as: A. Akbarzadeh-Sharbaf, V. Mohtashami and D. D. Giannacopoulos, "An Unconditionally Stable and Energy-Preserving Domain-Decomposition Method for Transient Modeling of Large-Scale Electromagnetic Problems," in IEEE Transactions on Antennas and Propagation, vol. 67, no. 11, pp. 6989-7000, Nov. 2019, doi: 10.1109/TAP.2019.2927844.

An Unconditionally Stable and Energy Preserving Domain Decomposition Method for Transient Modelling of Large-Scale Electromagnetic Problems

Ali Akbarzadeh-Sharbaf, Vahid Mohtashami, and Dennis D. Giannacopoulos, *Senior Member, IEEE*

***Abstract*—The purpose of this contribution is to introduce a dual-primal finite element tearing and interconnecting (DP-FETI) method for the time domain simulation of large electromagnetic problems. The most distinctive feature of the proposed method is that the continuity of the first time derivative of the electric field intensity is enforced across the interfaces, unlike the existing formulations in electromagnetics. A theoretical proof is provided to demonstrate that this transmission condition guarantees unconditional stability and energy preservation of the method. Since the condition number of the global interface problem is greatly reduced compared to the standard finite-element time-domain (FETD) method, an iterative solver converges in far fewer iterations. This significantly reduces simulation time, particularly when implemented on parallel computers. It is numerically shown that the method is scalable with respect to the number of subdomains and the time-step size. Numerical results for simulation of a cavity and bandgap devices are presented to demonstrate capability, accuracy, and efficiency of the proposed time-domain DP-FETI (TD-DP-FETI).**

***Index Terms*—Domain decomposition method, finite-element tearing and interconnecting (FETI), finite-element time-domain (FETD) method.**

I. Introduction

THE finite element tearing and interconnecting (FETI) method is one of the most powerful domain decomposition methods for simulation of large-scale problems and has successfully been applied to a wide range of applications in science and engineering, especially in the frequency domain. It first *tears* the problem into several non-overlapping subdomains and *interconnects* them together by solving a reduced global interface problem. Then, the solution is served as a boundary condition to compute the electric field inside each subdoamin. Breaking the initial problem into smaller subproblems not only decreases the computational cost but also makes the method amenable to parallel computing to gain further speedup. It was initially propsoed by Farhat and Roux in computational mechanics for elliptic equations [1]. The method was later improved by introducing the dula-primal (DP) FETI method [2]. The idea behind the method is to directly enforce the continuity condition for some degrees of freedom (DoFs) between the subdomains and employ a set of Lagrange multipliers (dual variables) to impose the continuity between the other DoFs across the subdomain interfaces. It was successfully applied to the Helmholtz equation in computational acoustics [3]. Different variations of the FETI have been extended to the second-order vector wave equation (VWE) in computational electromagnetics in the frequency domain [4]–[9]. It is shown that the DP-FETI is scalable with respect to the mesh size, the wavenumber and, importantly, the number of subdomains when the Dirichlet preconditioner is used to solve the global interface problem [3], [7]. However, further numerical studies revealed that the method does not exhibit satifactory numerical scalability when subdomains are larger than half of a wavelength. The reason was found to be the eigenspectrum of the left-hand side (LHS) matrix, which becomes indefinite for large subdomains [7]. A considerable improvement is observed when a Robin transmission condition is employed [8].

In contrast to the frequency-domain formulations, the time-domain (TD) counterparts have witnessed much less attention. The first TD-FETI methods were developed by Farhat [10], [11] and then adapted for electromagnetic problems based on the VWE equation [12]. However, it did not employ the dual-primal concept and no theoretical stability analysis has been performed. The TD-FETI has also been applied to multiphysics problems to couple electrical equations with other phenomena, such as thermal and mechanical; however, a simple current continuity equation was considered in the electrical part rather than Maxwell's equations. Moreover, the stability has not been studied theoretically [13], [14].

A large amount of work has been done on the TD-FETI methods for solving the equation of motion (a scalar wave-like equation) in structural dynamics [15]–[21]. The main focus has been on the development of stable and energy-preserving multi-time-step FETI algorithms in which each subdomain marches in time in its own time-step size. Hence, the time-step in each subdomain can be chosen such that it satisfies the accuracy and stability requirements of that subdomain. Gravouil [16] showed that imposing the first time derivative of the main variable (i.e. velocity) as the continuity condition guarantees stability and energy conservation of the method. The idea was used to develop a non-overlapping and stable hybrid finite-element-finite-differece formulation in the time domain [22]. Karimi [20] extended [16] to the multi-subdomain case by the aid of [17] without using the dual-primal concept. Subber [21] developed a formulation for non-matching grids. These formulations provide a controllable

Manuscript received ...

Ali Akbarzadeh-Sharbaf and Vahid Mohtashami are with the Faculty of Engineering, Ferdowsi University of Mashhad, Mashhad, Iran. Dennis D. Giannacopoulos is with the Department of Electrical and Computer Engineering, McGill University, Montréal, QC, Canada. (e-mail: v.mohtashami@um.ac.ir).

TD-FETI framework to efficiently and accurately capture the spatial and temporal scales of interest.

In this paper, we combine the DP-FETI method, extended to Maxwell's equations in the frequency domain in [7], with the advances that have been achieved in time-domain simulation of structural dynamics to develop a stable and energy-preserving DP-FETI method for transient modelling of large-scale electromagnetic problems (referred to as TD-DP-FETI). This formulation has the scalability properties of the DP-FETI method, converges much faster in comparison with the standard FETD when an iterative solver is applied, remains unconditionally stable, and preserves the total electromagnetic energy during time-stepping at the same time. The unconditional stability permits the user to choose the time-step size regardless of the stability issues. This property is of especial interest when the stability condition is very limiting, for example in low-frequency applications or when fine details are located on large structures [23]. The energy conservation property ensures that the total electromagnetic energy stored in the problem remains constant during simulation—obviously, in the absence of dissipative materials and boundary conditions and when impressed sources are off. This is important in applications that require high accuracy and energy conservation over long periods of time integration. Note that these two temporal properties are consequences of using the Newmark-β method with $\beta = 1/4$ and exist in the standard FETD. However, we demonstrate that they are retained when the TD-DP-FETI is applied, unlike the previous works in the electromagnetics community such as [12].

A Dirichlet transmission condition is preferred to a Robin transmission condition in this paper, as it guarantees positive definiteness of the global interface matrix for any problem. A Robin transmission condition would most likely yield a similar characteristic; however, the formulation and implementation become more complex and expensive. Moreover, unconditional stability and energy conservation properties of the method may not be preserved in that case.

The paper is organized as follows. The DP-FETI formulation and a few remarks on the implementation are given in Section II. Section III provides a detailed stability analysis. Finally, numerical results which demonstrate the validity, accuracy, and applicability of the proposed method are presented in Section IV.

II. Formulation

Let us consider a bounded computational space occupying domain Ω in $\mathbb{R}^3$ with boundary $\partial\Omega$ satisfying the Lipschitz condition. Moreover, let $\partial\Omega_{PEC}$, $\partial\Omega_{PMC}$, and $\partial\Omega_{ABC}$ respectively denote portions of the boundary on which perfect electrically conducting (PEC), perfect magnetically conducting (PMC), and absorbing boundary condition (ABC) boundary conditions are imposed ($\partial\Omega_{PEC} \cap \partial\Omega_{PMC} \cap \partial\Omega_{ABC} = \emptyset$). The transient behaviour of the electric field intensity $\boldsymbol{E}(\boldsymbol{r},t) : \Omega \times [0,T_f] \to \mathbb{R}^3, T_f > 0$ is governed by the VWE together with the boundary and initial conditions:

$$
\begin{aligned}
&\nabla \times \left(\mu^{-1}\nabla \times \boldsymbol{E}(\boldsymbol{r},t)\right) + \varepsilon\ddot{\boldsymbol{E}}(\boldsymbol{r},t) = -\dot{\boldsymbol{J}}_{imp}(\boldsymbol{r},t) && \text{in} \quad \Omega \times [0,T_f] \\
&\hat{n} \times \boldsymbol{E}(\boldsymbol{r},t) = 0 && \text{on} \quad \partial\Omega_{PEC} \times [0,T_f] \\
&\hat{n} \times \nabla \times \boldsymbol{E}(\boldsymbol{r},t) = 0 && \text{on} \quad \partial\Omega_{PMC} \times [0,T_f] \\
&\hat{n} \times c\nabla \times \boldsymbol{E}(\boldsymbol{r},t) + \hat{n} \times \hat{n} \times \dot{\boldsymbol{E}}(\boldsymbol{r},t) = 0 && \text{on} \quad \partial\Omega_{ABC} \times [0,T_f] \\
&\boldsymbol{E}(\boldsymbol{r},0) = \boldsymbol{E}_0 && \text{in} \quad \Omega, \\
&\dot{\boldsymbol{E}}(\boldsymbol{r},0) = \dot{\boldsymbol{E}}_0 && \text{in} \quad \Omega,
\end{aligned} \tag{1}
$$

where ε, μ, and c represent permittivity, permeability, and the speed of light in the medium, respectively; and $\boldsymbol{J}_{imp}(\boldsymbol{r},t)$ denotes an electric impressed current. A dot over a variable indicates a derivative taken with respect to time, which means $\dot{y} \equiv dy/dt$ and $\ddot{y} \equiv d^2y/dt^2$.

In order to apply the FETI method, the computational domain Ω is partitioned into N_s non-overlapping subdomains $\Omega^k; k = 1, \cdots, N_s$ ($\Omega = \cup_{k=1}^{N_s}\Omega^k, \quad \cap_{k=1}^{N_s}\Omega^k = \emptyset$) . Γ_k represents all the interfaces between subdomain k and its neighboring subdomains b_k. Among different continuity conditions that exist, the tangential continuity of the first time derivative of the electric field intensity across Γ_k is enforced here, as it guarantees unconditional stability and energy conservation of the method [16]. Note that the $\boldsymbol{E}$-continuity method has been discussed in the literature to be prone to instabilities [24], [25]. A drawback of the $\ddot{\boldsymbol{E}}$-continuity method is that there can be significant irrecoverable drift in $\boldsymbol{E}$ without employing constraint stabilization or projection methods [20]. The objective is to find the solution to (1) in every subdomain such that the given continuity condition is also satisfied. This constrained problem can be solved using the method of Lagrange multipliers. Let us first write the corresponding functional in each subdomain as [21], [26]

$$
\begin{aligned}
\mathcal{F}^k = \frac{1}{2}\int_{\Omega^k} \mu^{-1}\left(\nabla \times \boldsymbol{E}\right) \cdot \left(\nabla \times \boldsymbol{E}\right) dV \\
+ \frac{\varepsilon c}{2}\int_{\partial\Omega^k_{ABC}} \left(\hat{n} \times \boldsymbol{E}\right) \cdot \left(\hat{n} \times \dot{\boldsymbol{E}}\right) dS \\
+ \frac{1}{2}\int_{\Omega^k} \varepsilon\dot{\boldsymbol{E}} \cdot \dot{\boldsymbol{E}} dV + \int_{\Omega^k} \boldsymbol{E} \cdot \dot{\boldsymbol{J}}_{imp} dV.
\end{aligned} \tag{2}
$$

The weak form can be obtained by minimizing $\sum_{k=1}^{N_s}\mathcal{F}^k$ subject to

$$
\int_{\Gamma_k} \left(\dot{\boldsymbol{E}}_k - \dot{\boldsymbol{E}}_{b_k}\right) dS = 0 \quad ; \quad k = 1, 2, ..., N_s. \tag{3}
$$

This condition implies that the continuity of $\dot{\boldsymbol{E}}$ is enforced across all subdomain interfaces. Note that as we are dealing with conformal meshes in this paper, there is a one-to-one correspondence between unknowns residing on either side of Γ_k. Therefore, this constraint can be simplified to a boolean operation as will be discussed later. The Lagrangian for this minimization problem can be written as

$$
\Lambda = \sum_{k=1}^{N_s} \left(\mathcal{F}^k + \int_{\Gamma_k} \boldsymbol{\lambda} \cdot \left(\dot{\boldsymbol{E}}_k - \dot{\boldsymbol{E}}_{b_k}\right) dS\right) \tag{4}
$$

where $\boldsymbol{\lambda}$ is the Lagrange multiplier used to enforce the constraint. Taking the first variation of Λ, applying integration by parts, and then performing simplifications, we obtain

$$\int_{\Omega^k} \mu^{-1} \left(\nabla \times \boldsymbol{E}\right) \cdot \left(\nabla \times \boldsymbol{E}\right) dV + \int_{\Omega^k} \varepsilon \boldsymbol{E} \cdot \ddot{\boldsymbol{E}} dV + \varepsilon c \int_{\partial\Omega^k_{ABC}} \left(\hat{n} \times \boldsymbol{E}\right) \cdot \left(\hat{n} \times \dot{\boldsymbol{E}}\right) dS = - \int_{\Omega^k} \boldsymbol{E} \cdot \dot{\boldsymbol{J}}_{imp} dV - \int_{\Gamma_k} \boldsymbol{\lambda} \cdot \dot{\boldsymbol{E}}_k dS \quad (5a)$$

$$\int_{\Gamma_k} \left(\dot{\boldsymbol{E}}_k - \dot{\boldsymbol{E}}_{b_k}\right) dS = 0 \;\; ; \;\; k = 1, 2, ..., N_s. \quad (5b)$$

Expanding $\boldsymbol{E}$ in vector edge basis functions gives the following solution to the boundary value problem at $t = n\Delta t$

$$[\mathcal{S}^k]\{e^k\}^n + [\mathcal{R}^k]\{\dot{e}^k\}^n + [\mathcal{M}^k]\{\ddot{e}^k\}^n = \{f^k\}^n - [C^k_\star]\{\lambda\}^n \quad (6a)$$

$$\sum_{k=1}^{N_s} [C^k_\star]^T \{\dot{e}^k\}^n = \{0\} \quad (6b)$$

where $\{e^k\} = [e^k_1, e^k_2, ..., e^k_{N^k_{ed}}]^T$, $[C^k_\star]$ is a signed Boolean matrix to extract the unknowns residing on the interface in subdomain k, and

$$\mathcal{M}^k_{ij} = \int_{\Omega^k} \varepsilon \boldsymbol{N}_i \cdot \boldsymbol{N}_j dV \quad (7a)$$

$$\mathcal{R}^k_{ij} = \int_{\partial\Omega^k_{ABC}} Y \left(\hat{n} \times \boldsymbol{N}_i\right) \cdot \left(\hat{n} \times \boldsymbol{N}_j\right) dS \quad (7b)$$

$$\mathcal{S}^k_{ij} = \int_{\Omega^k} \mu^{-1} \nabla \times \boldsymbol{N}_i \cdot \nabla \times \boldsymbol{N}_j dV \quad (7c)$$

$$f^k_i(t) = - \int_{\Omega^k} \boldsymbol{N}_i \cdot \dot{\boldsymbol{\mathcal{J}}}_{imp}(t) dV \quad (7d)$$

in which $Y = \varepsilon c$ is the intrinsic admittance of the medium and $\boldsymbol{N}$ denotes the vector edge basis functions. Lossy materials can be simply included by adding the extra term $\int_{\Omega^k} \sigma \boldsymbol{N}_i \cdot \boldsymbol{N}_j dV$ to (7b). It should be noted that (6b) enforces continuity of the tangential component of $\dot{\boldsymbol{E}}$ across the interface, because $\boldsymbol{E}$ is expanded in terms of the edge basis functions. These basis functions guarantee tangential continuity of the electric field intensity [26].

In order to discretize (6a) in time, Newmark-β is the most commonly-used method, which involves [27]

$$\{e^k\}^{n+1} - \{e^k\}^n = \Delta t \{\dot{e}^k\}^n + \beta \Delta t^2 \{\ddot{e}^k\}^{n+1} + \Delta t^2 \left(\frac{1}{2} - \beta\right) \{\ddot{e}^k\}^n \quad (8a)$$

$$\frac{1}{\Delta t} \left(\{\dot{e}^k\}^{n+1} - \{\dot{e}^k\}^n\right) = \frac{1}{2} \left(\{\ddot{e}^k\}^{n+1} + \{\ddot{e}^k\}^n\right) \quad (8b)$$

where $0 \leq 2\beta \leq 1$. Note that $\beta = 1/4$ is the only value which yields second-order accuracy and unconditional stability simultaneously.

Equations (6a) and (8) can be combined together in a matrix form as

$$\begin{bmatrix} [\mathcal{M}^k] & [\mathcal{R}^k] & [\mathcal{S}^k] \\ -\frac{\Delta t}{2}[I] & [I] & [0] \\ -\beta \Delta t^2 [I] & [0] & [I] \end{bmatrix} \begin{bmatrix} \{\ddot{e}^k\} \\ \{\dot{e}^k\} \\ \{e^k\} \end{bmatrix}^{n+1} + \begin{bmatrix} [C^k_\star] \\ [0] \\ [0] \end{bmatrix} \{\lambda\}^{n+1} = \begin{bmatrix} \{f^k\}^{n+1} \\ \{\dot{e}^k\}^n + \frac{\Delta t}{2}\{\ddot{e}^k\}^n \\ \{e^k\}^n + \Delta t \{\dot{e}^k\}^n + \Delta t^2 \left(\frac{1}{2} - \beta\right) \{\ddot{e}^k\}^n \end{bmatrix} \quad (9)$$

or compactly:

$$[H^k]\{U^k\}^{n+1} + [C^k]\{\lambda\}^{n+1} = \{b^k\}^n. \quad (10)$$

Solving (10) together with the continuity condition (6b) gives the solution to every subdomain.

The formulation explained above can treat multiple subdomains as long as the interfaces between the subdomains (Γ_k's) do not cross each other. In order to relax this restriction, we first partition the unknown vector in each subdomain $\{e^k\}$ into two parts such that

$$\{e^k\} = \{ \;\; \{e^k_r\}^T \;\; \{e^k_c\}^T \;\; \}^T \quad (11)$$

where $\{e^k_c\}$ represents the corner unknowns, those shared among more than two subdomains, and $\{e^k_r\}$ contains the *remainder*. Applying this partitioning scheme, (10) can be written as

$$\begin{bmatrix} [H^k_{rr}] & [H^k_{rc}] \\ [H^k_{cr}] & [H^k_{cc}] \end{bmatrix} \begin{bmatrix} \{U^k_r\} \\ \{U^k_c\} \end{bmatrix}^{n+1} + \begin{bmatrix} [C^k_r] \\ [0] \end{bmatrix} \{\lambda\}^{n+1} = \begin{bmatrix} \{b^k_r\} \\ \{b^k_c\} \end{bmatrix}^n \quad (12)$$

in which $[C^k_r]^T = [[C^k_{\star r}]^T \; [0] \; [0]]^T$. It is worth mentioning that $[C^k_{\star r}]$ contains all the information of $[C^k_\star]$, as we assumed there are no cross-points, thus no corner edges, in the derivation of $[C^k_\star]$. As can be seen from (12), no Lagrange multipliers are defined for corner DoFs, because the continuity is enforced in the same way as the internal unknowns. All corner DoFs across the computational domain are merged and defined through the global vector $\{e_c\}$. This is achieved by introducing another signed Boolean matrix in every subdomain, denoted by $[B^k_c]$, which relates local to global corner unknowns by $\{e^k_c\} = [B^k_c]\{e_c\}$. Now, the global system becomes

$$\begin{bmatrix} [H^1_{rr}] & \cdots & [0] & [H^1_{rc}][\hat{B}^1_c] & [C^1_r] \\ \vdots & \ddots & \vdots & \vdots & \vdots \\ [0] & \cdots & [H^{N_s}_{rr}] & [H^{N_s}_{rc}][\hat{B}^{N_s}_c] & [C^{N_s}_r] \\ [\hat{B}^1_c]^T[H^1_{cr}] & \cdots & [\hat{B}^{N_s}_c]^T[H^k_{rc}] & [H_{cc}] & [0] \\ [B^1_r] & \cdots & [B^{N_s}_r] & [0] & [0] \end{bmatrix} \begin{bmatrix} \{U^1_r\} \\ \vdots \\ \{U^{N_s}_r\} \\ \{U_c\} \\ \{\lambda\} \end{bmatrix}^{n+1} = \begin{bmatrix} \{b^1_r\} \\ \vdots \\ \{b^{N_s}_r\} \\ \{b_c\} \\ \{0\} \end{bmatrix}^n \quad (13)$$

where $[B^k_r] = [\;[0] \;\; [C^k_{\star r}]^T \;\; [0]\;]$, $[\hat{B}^k_c] = diag([B^k_c], [B^k_c], [B^k_c])$, $\{b_c\} = \sum_{k=1}^{N_s} [\hat{B}^k_c]^T \{b^k_c\}$, and

$[H_{cc}] = \sum_{k=1}^{N_s} [\hat{B}_c^k]^T [H_{cc}^k][\hat{B}_c^k]$. Solving (13) for $\{\lambda\}$, yields

$$[\mathcal{R}_\lambda]\{\lambda\}^{n+1} = \{d_r\}^n - [\mathcal{F}_{rc}][\tilde{\mathcal{K}}_{cc}]^{-1}\{\tilde{f}_c\}^n \tag{14}$$

in which

$$[\mathcal{R}_\lambda] = [\mathcal{F}_{rr}] + [\mathcal{F}_{rc}][\tilde{\mathcal{K}}_{cc}]^{-1}[\mathcal{F}_{cr}] \tag{15}$$

$$[\mathcal{F}_{rr}] = \sum_{k=1}^{N_s} [B_r^k][H_{rr}^k]^{-1}[C_r^k] \tag{16}$$

$$[\mathcal{F}_{rc}] = \sum_{k=1}^{N_s} [B_r^k][H_{rr}^k]^{-1}[H_{rc}^k][\hat{B}_c^k] \tag{17}$$

$$[\mathcal{F}_{cr}] = \sum_{k=1}^{N_s} [\hat{B}_c^k]^T[H_{cr}^k][H_{rr}^k]^{-1}[C_r^k] \tag{18}$$

$$\{\tilde{f}_c\}^n = \{b_c\}^n - \sum_{k=1}^{N_s} [\hat{B}_c^k]^T[H_{cr}^k][H_{rr}^k]^{-1}\{b_r^k\}^n \tag{19}$$

$$\{d_r\}^n = \sum_{k=1}^{N_s} [B_r^k][H_{rr}^k]^{-1}\{b_r^k\}^n \tag{20}$$

$$[\tilde{\mathcal{K}}_{cc}] = [H_{cc}] - \sum_{k=1}^{N_s} [\hat{B}_c^k]^T[H_{cr}^k][H_{rr}^k]^{-1}[H_{rc}^k][\hat{B}_c^k]. \tag{21}$$

Once the Lagrange multiplier is computed, the solution to the global corner unknowns can be computed by

$$[\tilde{\mathcal{K}}_{cc}]\{U_c\}^{n+1} = \{\tilde{f}_c\}^n + [\mathcal{F}_{cr}]\{\lambda\}^{n+1}. \tag{22}$$

Finally, solving (12) gives the electric field intensity at $t = (n+1)\Delta t$ in every subdomain. This process has to be repeated until the end of the simulation.

This approach reduces the cost of solving the original system of equations arising from the standard FETD to that of a series of smaller systems the most cumbersome of which is (14). As the global interface problem is 2-D by nature, it has far fewer unknowns compared to the original 3-D system of equations. Moreover, it converges much faster than the FETD, because it has a better condition number.

Before moving on to the stability analysis, a few remarks on the formulation and implementation should be pointed out:

• A block matrix notation is followed in the derivation for the sake of brevity. However, this should be avoided in the implementation. Because this not only triples the size of the matrices but also destroys their symmetry. The above equations should be further expanded and simplified.

• Each time step involves solving three major systems of equations, namely (14), (22), and (12)—the last one has to be solved for each and every subdomain. As the LHS matrices are time-independent and the solving process has to be repeated every time step, it would be more efficient to employ a direct solver as long as the matrices are not very large in size, which is often the case. A direct solver factorizes the LHS matrix $[A]$ once before the time-stepping loop. Then, solving $[A][X] = [B]$ during time-stepping involves only forward-backward substitution, which is a very low-cost operation. This is usually feasible for (12) and (22), but not for (14). Because $[\mathcal{R}_\lambda]$ is a dense matrix. In order to further study this, let us first expand the LHS matrix of (14), which gives

$$[\mathcal{R}_\lambda] = \frac{\Delta t}{2}[\mathcal{F}_{rr}] + \frac{\Delta t}{2}[\hat{\mathcal{F}}_{rc}]\left(\sum_{k=1}^{N_s}[B_c^k]^T[\mathbb{S}^k][B_c^k]\right)[\hat{\mathcal{F}}_{rc}]^T \tag{23}$$

where $[\mathcal{F}_{rr}] = \sum_{k=1}^{N_s}[C_{\star r}^k]^T[\mathcal{Q}_{rr}^k]^{-1}[C_{\star r}^k]$, $[\mathcal{Q}^k] = [\mathcal{M}^k] + \frac{\Delta t}{2}[\mathcal{R}^k] + \beta\Delta t^2[\mathcal{S}^k]$, and $[\hat{\mathcal{F}}_{rc}] = \sum_{k=1}^{N_s}[C_{\star r}^k]^T[\mathcal{Q}_{rr}^k]^{-1}[\mathcal{Q}_{rc}^k][B_c^k]$. $[\mathbb{S}^k] = [\mathcal{Q}_{cc}^k] - [\mathcal{Q}_{cr}^k][\mathcal{Q}_{rr}^k]^{-1}[\mathcal{Q}_{rc}^k]$ is the Schur complement of $[\mathcal{Q}_{rr}^k]$ in $[\mathcal{Q}^k]$. Factorization of $[\mathcal{R}_\lambda]$ requires a large amount of memory for not very large 3-D problems. The common remedy is to load the matrix in memory part-by-part, but this slows down the operation considerably. Therefore, an iterative solver may often be employed. As $[\mathcal{M}^k]$ is positive definite (PD) and $[\mathcal{R}^k]$ and $[\mathcal{S}^k]$ are positive semi-definite, $[\mathcal{Q}^k]$ is PD. It is also well-known that for a 2×2 block matrix with square diagonal blocks, e.g. $[\mathcal{Q}^k]$, its Schur complements and both diagonal blocks are PD if and only if the matrix itself is PD. Therefore, $[\mathcal{Q}_{rr}^k]$, $[\mathcal{Q}_{cc}^k]$, and $[\mathbb{S}^k]$ are all PD. Hence, it can be concluded that $[\mathcal{R}_\lambda]$ is PD and symmetric—because all submatrices are symmetric. The conjugate gradient (CG) method is thus a suitable candidate to solve such systems iteratively [28]. Although it is well-known that the covergence of the CG method for PD matrices is guaranteed [28], a preconditioner is often employed to accelerate its convergence. The optimal one for the DP-FETI is the Dirichlet preconditioner [29], which can be written as

$$[\mathcal{F}_{rr}^D]^{-1} = \sum_{k=1}^{N_s}[C_{\star r}^k]^T \begin{bmatrix}[0] & [0]\\ [0] & [\mathbb{S}_{II}^k]\end{bmatrix}[C_{\star r}^k] \tag{24}$$

where $[\mathbb{S}_{II}^k] = [Q_{II}^k] - [Q_{IV}^k][Q_{VV}^k]^{-1}[Q_{VI}^k]$. The subscripts I and V refer to the *interface* (dual unknowns) and *Volume* (non-interface) DoFs. It can be shown that $[\mathcal{F}_{rr}^D]^{-1}$ is a good approximation of $[\mathcal{F}_{rr}]^{-1}$ [29].

• The FETI consumes more memory than the standard finite element method, as it involves computation of extra matrices. This statement holds for the proposed TD-DP-FETI as well. However, following some simple tips can keep the extra memory usage at a minimum. The memory usage is also dominated by solving the three aforementioned systems of equations. The FETI is known to be especially efficient for periodic structures such as antenna arrays and bandgap devices. For such problems, solving the subdomain problem (12) requires storing matrices for only several subdomains with unique characteristics. The number of these subdomains is almost independent of the array size. The corresponding LHS matrices can be factorized in the preprocessing step to improve efficiency. The size of the global corner matrix $[\tilde{\mathcal{K}}_{cc}]$ remains fairly small for a medium-sized array and, hence, it can be also factorized to solve the corner problem (22) at low cost. For very large problems, this matrix is still orders of magnitude smaller than the total number of unknowns. Due to high memory usage, $[\mathcal{R}_\lambda]$ cannot even be fully assembled and the global interface problem (14) is usually solved iteratively by the CG method. The matrix-vector multiplications in each

iteration mainly require the unique matrices already stored in memory. $[\mathcal{R}_\lambda]$ can be constructed on the fly during the CG method, thereby evading the storage requirements for it.

• Due to tremendous memory usage, explicit inversion of matrices must be avoided at all cost. For example, in order to compute $[Y] = [B][A]^{-1}[B]$, one should first compute $[X]$ by solving $[A][X] = [B]$ system. Then $[Y]$ is given by $[B][X]$. Since $[A]$ belongs to subdomains and it is usually prefactorized, computing $[Y]$ would be very cheap. If $[B]$ is the product of several matrices, the order of operations has to be chosen such that the computation cost is minimized.

III. Stability Analysis

In this section, stability of the proposed TD-DP-FETI formulation is studied for $\beta = 1/4$. It is shown that the method retains the fundamental properties of the standard FETD formulation discretized using the Newmark-β method, i.e., unconditionally stability and energy conservation. This means that the interface condition does not deteriorate the stability condition. The stability analysis is performed based on the energy method, which is a powerful technique that has been used in different engineering disciplines for a long time [30]. Let us first define the following operators

$$[\![x^n]\!] = x^{n+1} - x^n \tag{25a}$$

$$\langle\!\langle x^n \rangle\!\rangle = x^{n+1} + x^n. \tag{25b}$$

The Newmark-β relations (8) can be rewritten in an alternative form, given by

$$\langle\!\langle \{\dot{e}^k\}^n \rangle\!\rangle = \frac{2}{\Delta t} [\![\{e^k\}^n]\!] + \Delta t(0.5 - 2\beta) [\![\{\ddot{e}^k\}^n]\!] \tag{26a}$$

$$\langle\!\langle \{\ddot{e}^k\}^n \rangle\!\rangle = \frac{2}{\Delta t} [\![\{\dot{e}^k\}^n]\!]. \tag{26b}$$

It is well-known that for any symmetric matrix $[A]$, the following identity holds

$$\langle\!\langle x^n \rangle\!\rangle^T [A] [\![x^n]\!] = [\![x^n]\!]^T [A] \langle\!\langle x^n \rangle\!\rangle = [\![(x^n)^T [A] x^n]\!]. \tag{27}$$

Summing (6a) over two consecutive time steps and premultiplying it by $\langle\!\langle \{\dot{e}^k\}^n \rangle\!\rangle^T$ yields

$$\begin{aligned} &\langle\!\langle \{\dot{e}^k\}^n \rangle\!\rangle^T [\mathcal{S}^k] \langle\!\langle \{e^k\}^n \rangle\!\rangle + \langle\!\langle \{\dot{e}^k\}^n \rangle\!\rangle^T [\mathcal{R}^k] \langle\!\langle \{\dot{e}^k\}^n \rangle\!\rangle + \\ &\langle\!\langle \{\dot{e}^k\}^n \rangle\!\rangle^T [\mathcal{M}^k] \langle\!\langle \{\ddot{e}^k\}^n \rangle\!\rangle = -\langle\!\langle \{\dot{e}^k\}^n \rangle\!\rangle^T \begin{bmatrix} [C^k_{\star r}] \\ [0] \end{bmatrix} \langle\!\langle \{\lambda\}^n \rangle\!\rangle \end{aligned} \tag{28}$$

in which the source term has been removed, as it does not affect the stability analysis. Note that the matrices and unknown vectors in (28) are partitioned in the same way as in (12). Moreover, as $[\mathcal{R}^k]$ is positive semi-definite, $r^n_k = \langle\!\langle \{\dot{e}^k\}^n \rangle\!\rangle^T [\mathcal{R}^k] \langle\!\langle \{\dot{e}^k\}^n \rangle\!\rangle \geq 0$. Replacing the second time derivative terms in (28) by (26b) and the first $\{\dot{e}^k\}$ term by (26a), (28) becomes

$$\begin{aligned} &[\![\mathscr{E}^n_{e_k}]\!] + [\![\mathscr{E}^n_{m_k}]\!] \\ &\quad + 0.25\Delta t^2 (0.5 - 2\beta^k) [\![\{\ddot{e}^k\}^n]\!]^T [\mathcal{S}^k] \langle\!\langle \{e^k\}^n \rangle\!\rangle \\ &+ (0.25\Delta t) r^n_k = -0.25\Delta t \langle\!\langle \{\dot{e}^k\}^n \rangle\!\rangle^T \begin{bmatrix} [C^k_{\star r}] \\ [0] \end{bmatrix} \langle\!\langle \{\lambda\}^n \rangle\!\rangle \end{aligned} \tag{29}$$

where

$$\mathscr{E}^n_{e_k} = \frac{1}{2} \left(\{\dot{e}^k\}^n\right)^T [\mathcal{M}^k] \{\dot{e}^k\}^n \tag{30a}$$

$$\mathscr{E}^n_{m_k} = \frac{1}{2} \left(\{e^k\}^n\right)^T [\mathcal{S}^k] \{e^k\}^n \tag{30b}$$

are defined as the energy stored in subdomain k due to the electric field and magnetic field at $t = n\Delta t$, respectively. The summation of (29) over all subdomains causes the right-hand side to vanish due to the continuity condition (6b). As $r^n_k \geq 0$, it can be immediately seen that

$$\mathscr{E}^{n+1}_{e_t} + \mathscr{E}^{n+1}_{m_t} \leq \mathscr{E}^n_{e_t} + \mathscr{E}^n_{m_t} \tag{31}$$

where the subscript "t" implies the total energy stored in all subdomains. This shows that the total stored electromagnetic energy decreases during time-stepping for any Δt, which proves unconditional stability of the method. In the absence of $[\mathcal{R}^k]$, r^k_n vanishes and the inequality in (31) changes to equality. This demonstrates that the method not only is unconditionally stable but also preserves the total energy. This will be numerically verified in Section IV-A.

IV. Numerical Studies

In this section, four numerical examples are presented to show the validity and effectiveness of the proposed method. Each example is designed such that some important characteristics of the method are also demonstrated.

Linear basis functions and $\beta = 1/4$ are used in all simulations, unless otherwise mentioned. The electric field distributions are visualized by ParaView [31]. Simulations are performed on a PC equipped with an Intel Core i7-4790K CPU and 32 GB of memory. The CG method with stopping criterion of 10^{-12} is employed to solve the global interface problem except for the first example (the cavity problem) in which a direct solver is used. The initial guess vector is assumed to be zero in every time step for the CG method.

A. Brick-Shaped Cavity

A 2cm×2cm×1cm brick-shaped cavity is divided into four 1cm×1cm×1cm cubic subdomains. A PEC boundary condition is enforced on all exterior walls. The domain is first discretized by cubic elements with edge length $h = 1mm$; then, each cube is divided into 6 tetrahedra. The time-step size is set to the upper bound of the stability condition of the Newmark-β method for $\beta = 0$. This condition can be obtained by rewriting the corresponding discretized VWE in the form $\{e\}^{n+1} = [A]\{e\}^n$. $[A]$, known as the amplification matrix, shows the growth of the solution over one step. For a stable

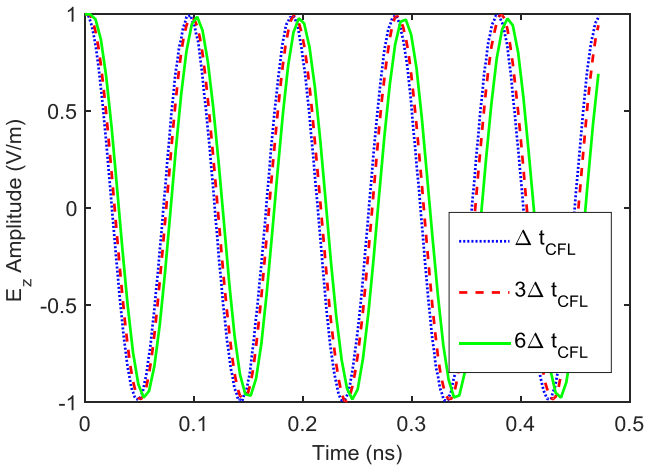

Fig. 1. E_z in the center of the cavity recorded over 5 periods for three different values of $\Delta t = \Delta t_{CFL}, 3\Delta t_{CFL}, 6\Delta t_{CFL}$. The time shifts are due to the insufficient resolution, which has led to numerical dispersion error.

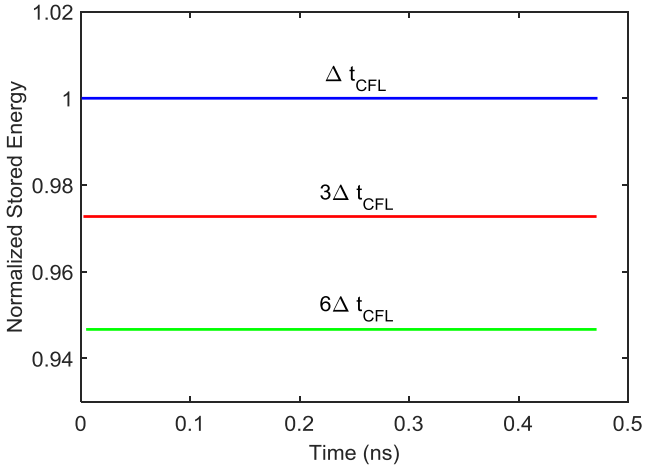

Fig. 2. Total discrete electromagnetic energy stored in the cavity computed for three different values of $\Delta t = \Delta t_{CFL}, 3\Delta t_{CFL}, 6\Delta t_{CFL}$. The discrete energy is perfectly preserved during time-stepping. The results are normalized with respect to the Δt_{CFL} case.

solution, eigenvalues of $[A]$ must be within the unit circle, i.e. $|\lambda_A| \leq 1$. Applying this condition gives

$$\Delta t_{CFL} = \frac{2}{\sqrt{\rho\left([\mathcal{M}]^{-1}[\mathcal{S}]\right)}} \simeq 8.182 \times 10^{-13} \text{ s} \qquad (32)$$

where $\rho(\cdot)$ is the spectral radius of $(\cdot)$. This approach ensures that the chosen time-step size is small enough to accurately capture field variations—this criterion is only applicable to small problems due to the computation cost of (32). The electric field distribution at the dominant mode (TM^z_{110}) with unit amplitude is projected on the mesh and used as the initial condition of the problem.

Fig. 1 shows the z component of the electric field intensity in the center of the cavity recorded over 5 periods for three different values of $\Delta t = \Delta t_{CFL}, 3\Delta t_{CFL}, 6\Delta t_{CFL}$. The results are completely stable and match with the theoretical solution (i.e., sinusoidal). Larger Δt's are also tested, but no sign of instability is observed. It should be noted that the time shifts between the curves are due to the numerical dispersion error. This problem worsens as the time-step size increases.

Variations of the total discrete electromagnetic energy ($\mathscr{E}^n_{em_t} = \mathscr{E}^n_{e_t} + \mathscr{E}^n_{m_t}$) stored in the cavity over the same time window for similar time steps are plotted in Fig. 2. It shows that the proposed method exactly preserves the discrete electromagnetic energy of the problem, as proved before. The results are normalized to the solution for Δt_{CFL}. Small changes in the energy levels are due to the variations in $\{e\}$ and $\{\dot{e}\}$ because of the temporal discretization error. This phenomenon can also be observed in Fig. 1 where electric field amplitude slowly diminishes as the time-step size increases.

Fig. 3 shows the eigenspectra of the global interface matrix. The system possesses only real positive eigenvalues for different Δt's, which verifies positive definiteness of $[\mathcal{R}_\lambda]$.

Finally, the electric field distribution at the last time step is depicted in Fig. 4 which closely resembles the TM^z_{110} mode field pattern.

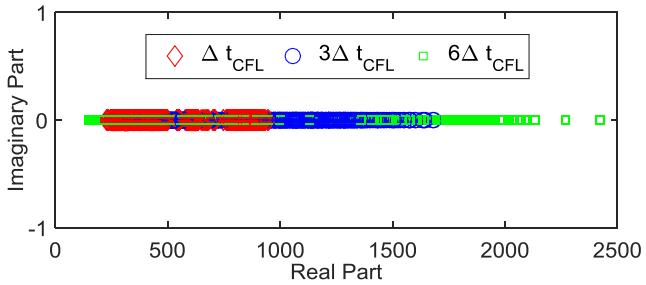

Fig. 3. Eigenspectra of the global interface matrix of the cavity problem for three different values of $\Delta t = \Delta t_{CFL}, 3\Delta t_{CFL}, 6\Delta t_{CFL}$.

B. Photonic Crystal Cavity

Metamaterials are engineered materials having unique electromagnetic properties not observed in bulk materials. These properties are derived from their periodic structures rather than characteristics of the base materials. They are divided into different classes depending on the properties they exhibit. One important class is bandgap structures such as electromagnetic bandgap (EBG) and photonic crystals. Propagation of electromagnetic waves over certain frequency bands, known as bandgaps, is prohibited through these structures. Another interesting feature is that introducing a defect, for example by removing a unit cell, in an otherwise perfect crystal could create a cavity within its bandgap from which the light cannot escape, if the cavity has proper size to support the mode. In the next two examples, the performance of the proposed TD-DP-FETI method by simulating these structures is studied.

As shown in Fig. 5, a square lattice photonic crystal structure composed of 11×11 dielectric rods residing on an infinite ground plane is considered for this example [32]. The lattice constant (spatial period) is denoted as a in both directions. The rods are $1.6a$ in height, $0.18a$ in radius, and have a relative permittivity of 11.56. A defect is made by replacing the central rod by a monopole antenna fed by an air-filled coaxial port. The monopole has a radius of $0.1a$ and height of $0.8a$. The inner and outer radii of the coaxial port

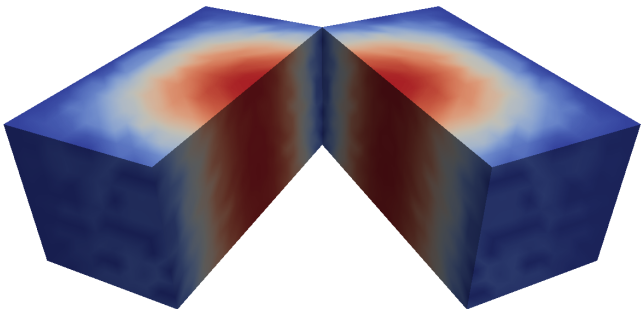

Fig. 4. Distribution of $|E|$ of the cavity problem at the last time step. The cavity is cut open for better visibility.

are $0.1a$ and $0.23a$, respectively. The monopole is excited by a modulated Blackman-Harris window with a central frequency of f_m = 11 GHz and half bandwidth of 5 GHz. The time-step size is set to one-300th of the window width to provide a smooth discrete signal. $a = 0.01$ m is chosen so the crystal exhibits the same behaviour in microwave frequencies. Each unit cell is considered as a subdomain in the TD-DP-FETI implementation. Mesh generation produced 44,712 unknowns per subdomain, 2000 corner, and 130,600 dual unknowns in total. The reference solution is obtained by solving the problem using the standard FETD formulation on the same mesh (with more than 5.27M unknowns). The CG method solved the global interface problem in 23 iterations while it converged after 228 iterations in the standard FETD (without preconditioning).

A comparison between the transient reflected voltage recorded at the coaxial port computed by the proposed TD-DP-FETI and the standard FETD, as the reference, has been drawn in Fig. 6. The absolute error between these two is plotted as an inset. The error is very small, almost on the order of machine precision of the computational hardware.

The magnitude of the reflection coefficient is plotted in Fig. 7 versus frequency. There is clearly a bandgap around 10.5 GHz. In order to further study the phenomenon, the simulation is repeated twice. The Gaussian pulse is replaced by 10.5 GHz and 15.15 GHz sinusoidal waveforms, lying inside and outside the bandgap, respectively. Fig. 8 shows the distribution of E_z-field on the ground (PEC) plane at these two frequencies. The field is confined to the vicinity of the cavity at 10.5 GHz while propagates through the structure at 15.15 GHz.

C. EBG Structure

This example involves simulation of an EBG structure, which is a modified version of what is proposed in [33]. The EBG is made of circular-section Alumina rods of radius 2 mm and $\varepsilon_r = 9.4$ oriented along the z-axis (see Fig. 9 for a unit cell). The rods form an $m_x \times m_y$ rectangular lattice with the lattice constant equal to 7 mm and are 3 cm in height. A PEC boundary condition is imposed on the top and bottom planes (parallel to the xy-plane) while the remaining four side walls are terminated by a first-order ABC. A z-polarized plane-wave with unit amplitude travelling in the $+x$ direction is

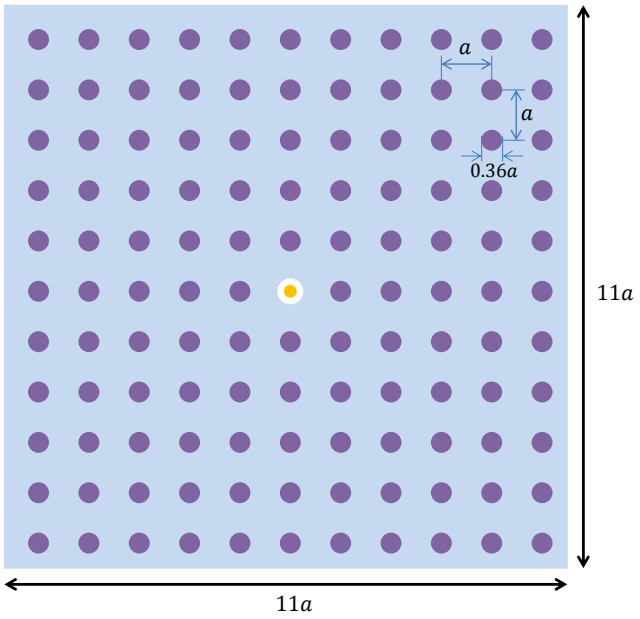

Fig. 5. The photonic crystal structure is made of 11×11 dielectric rods residing on an infinite ground plane (shown in light blue). The lattice constant is equal to a in both directions. The cavity is created and excited by replacing the central rod by a monopole antenna.

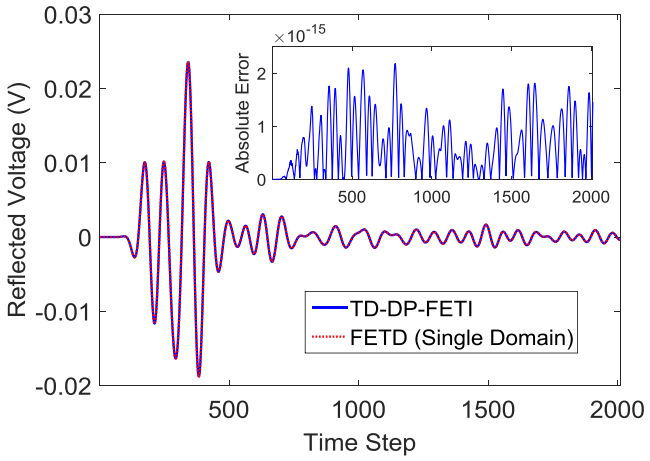

Fig. 6. Time-domain reflected voltages recorded at the excitation port computed by the proposed TD-DP-FETI method and the conventional FETD on the same mesh. The inset shows the absolute error between the results.

incident on the structure. It has a sinusoidal waveform with $f_0 = 12$ GHz. Each unit cell, considered as a subdomain in the TD-DP-FETI implementation, is discretized by tetrahedral elements with maximum edge length of 1 mm yielding 17,066 unknowns.

The scalability of the DP-FETI has been studied multiple times in the frequency domain [3], [7], [8]. It is shown that the method is scalable with respect to the mesh size, the subdomain size, the number of subdomains, and the wavenumber when equipped with the Dirichlet preconditioner. This is especially true when the ratio of the subdomain length to the wavelength is smaller than one half. As for the proposed TD-DP-FETI, although a simple Dirichlet transmission condition is used to couple the subdomains, a better scalability is

TABLE I
AVERAGE NUMBER OF THE CG ITERATIONS AND AVERAGE ELAPSED TIME PER CG ITERATION REQUIRED TO SOLVE THE GLOBAL INTERFACE PROBLEM FOR DIFFERENT EBG SIZES (STOPPING CRITERION = 10^{-12}). THE SIMULATION IS PERFORMED FOR TWO DIFFERENT TIME-STEP SIZES.

	Time-step size	Preconditioning	EBG size					
			5×5	10×10	15×15	20×20	25×25	30×30
Average No. of CG iterations	$\Delta t_0 = T_0/30$	✗	31	30	30	30	30	30
		✓	7	7	7	7	7	7
	$\Delta t_1 = 5\Delta t_0$	✗	128	128	128	128	128	128
		✓	15	15	15	15	15	15
Average elapsed time per CG iteration (s)		✗	0.23	0.86	1.96	3.44	5.38	7.49
		✓	0.30	1.20	2.74	4.79	7.48	10.73
Total number of unknowns			426,650	1,706,600	3,839,850	6,826,400	10,666,250	15,359,400
Total number of dual unknowns			24,760	110,340	256,620	463,600	731,280	1,059,660
Total number of corner unknowns			480	2,430	5,880	10,830	17,280	25,230

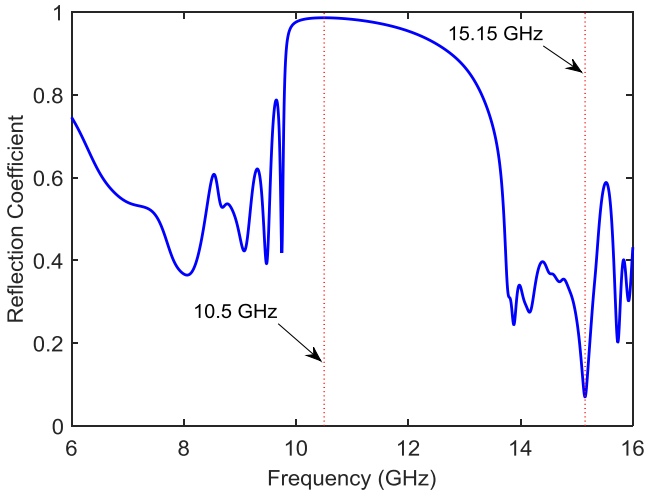

Fig. 7. The magnitude of the reflection coefficient of the photonic crystal cavity as a function of frequency plotted over 6-16 GHz. 10.5 GHz and 15.15 GHz frequencies lie inside and outside the bandgap, respectively.

expected compared to a frequency-domain DP-FETI as $[\mathcal{R}_\lambda]$ is always PD. Hence, we only investigate the effect of the two most important parameters, e.g. number of subdomains and time-step size, on the scalability. The time-step in the TD-DP-FETI plays a similar role to the wavenumber in the frequency-domain DP-FETI in shifting the eigenvalues of the system. However, the former shifts them to the right and keeps it always PD while the latter shifts them to the left and might make it indefinite.

In order to assess the scalability of the proposed method, we assumed the lattice to be square ($m_x = m_y$). One empty cell is considered immediately next to the ABC, so the total number of rods in the problem is $(m_x-2)^2$. The simulation is performed for two time-step sizes $\Delta t_0 = T_0/30$ ($T_0 = 1/f_0$) and $\Delta t_1 = 5\Delta t_0$. The size of the EBG is then progressively increased and the average number of the CG iterations and the average time taken to complete one CG iteration to solve the global interface problem is recorded during time-stepping. Since the computational cost of time-stepping is dominated by the solution of the interface problem, iteration count is a good measure to evaluate efficiency of the method. The average elapsed time for different Δt's are very close together and therefore only one of them is reported. The simulation statistics are tabulated in Table I. The proposed method exhibits an excellent numerical scalability property with respect to the EBG size ranging from 5×5 to 30×30 for a given Δt, even when the preconditioning is not applied. However, scalability of the method with respect to the time-step size is not as ideal. As the time-step size increases from Δt_0 to Δt_1, a rise in the CG iteration count from 30 to 128 is observed in the absence of preconditioning. Applying the Dirichlet preconditioner not only significantly accelerates the CG convergence rate (to 7 and 15 iterations for Δt_0 and Δt_1 respectively) but also dramatically improves the scalability of the TD-DP-FETI with respect to Δt. Regarding the computation time, although applying the Dirichlet preconditioner makes each CG iteration longer, it decreases the total CPU time by decreasing the number of CG iterations.

Another noteworthy observation is that the scalability of the proposed TD-DP-FETI with respect to the subdomain size is quite similar to its scalability with respect to Δt^{-1}. For example, if the lattice constant and the time-step size are set to $0.2a$ and Δt_0, respectively, similar results to those reported in Table I for Δt_1 will be obtained. This is due to the fact that varying the frequency of the source, which changes the subdomain size relative to the wavelength, does not directly affect the LHS matrix in FETD and the global interface problem in TD-DP-FETI. However, the time-step size must be accordingly modified to provide sufficient temporal resolution. Our numerical studies have confirmed this phenomenon but are not reported here.

In order to validate the solution, we consider a 20×8 array around which four empty unit cells are added to keep the ABC far from the rods to improve its performance (28×16 cells in total) [33]. The problem yields 519,684 dual, 12,150 corner, and 7,645,568 total unknowns. The simulation is continued until $t = 1350\Delta t_0$ when it reaches steady state. Fig. 10 shows distribution of the electric field amplitude $|E|$ over the plane passing trough the middle of the rods. The EBG does not allow the plane-wave to pass through, as f_0 falls in the structure bandgap. The convergence history for solving the global interface problem at the last time step, i.e. at $t = 1350\Delta t_0$, for both time steps is plotted in Fig. 11. The CG converged at exactly the same number of iterations as those reported in Table I. Each CG iteration took 5.75 s and 3.98 s to complete in the preconditioned and non-preconditioned cases,

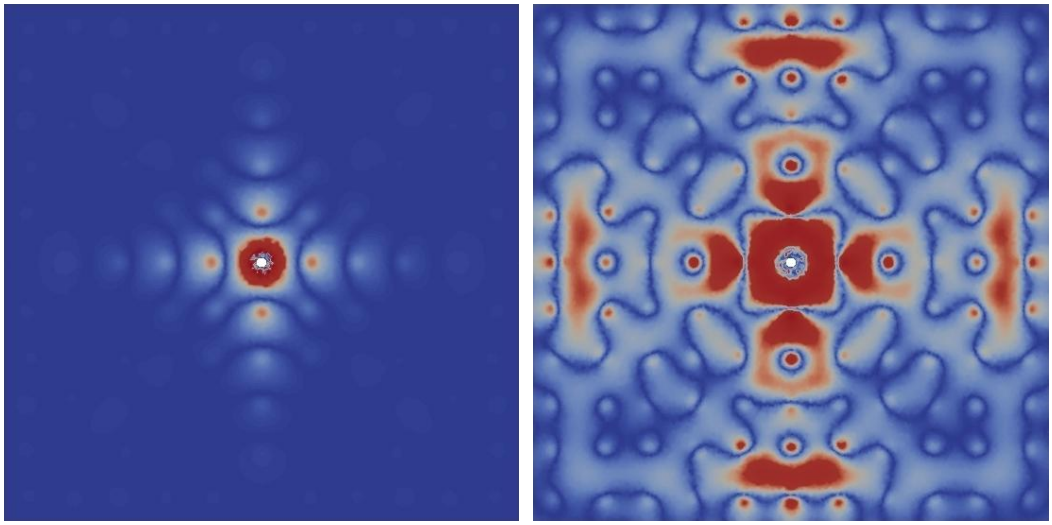

Fig. 8. E_z-field distribution on the PEC plane of the photonic crystal cavity at two different frequencies: (a) 10.5 GHz; and (b) 15.15 GHz. The field is confined to the vicinity of the cavity at 10.5 GHz while propagates through the structure at 15.15 GHz.

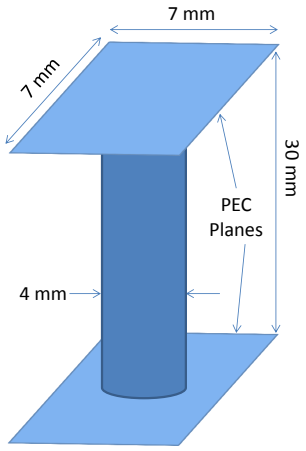

Fig. 9. A unit cell of the EBG structure.

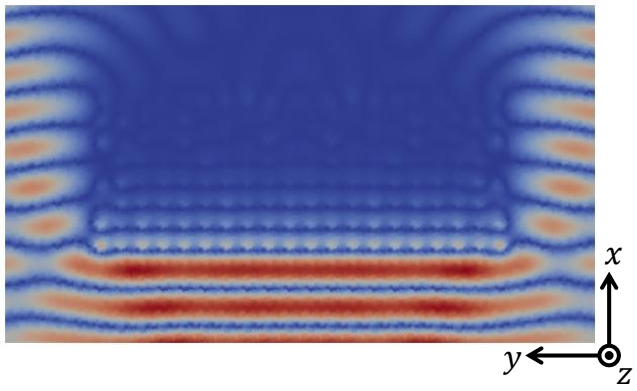

Fig. 10. Electric field distribution across the 8×20 EBG structure surrounded by 4 layers of empty cells after reaching steady state. The plane-wave cannot propagate through the lattice when its frequency lies in the EBG bandgap.

respectively.

D. Periodic Array of Double-Cones

The last example is considered to measure the performance of the proposed TD-DP-FETI against the standard FETD. The problem is a periodic structure similar to the previous example. However, the unit cell height is reduced to 10 mm and the rods are replaced by dielectric double-cones (see Fig. 12). They are 8 mm in height and 4 mm in width. They are placed in the center of the unit cells and have $\varepsilon_r = 10$. Each unit cell is discretized by 11,760 tetrahedra yielding 14,783 unknowns. Sharp tips of the double-cone require a very fine discretization of the mesh to adequately resolve the singularities. The ratio of the longest edge to the shortest edge in the mesh is around 150. The excitation is similar to the previous example. Simulations are carried out for 10×10, 20×20, and 30×30 arrays and time-step size is Δt_0. To make a fair comparison, preconditioning is not applied.

The computational statistics of the standard FETD and TD-DP-FETI for various array sizes are given in Table II. The results show that both methods have very good scalability with respect to the array size. This is due to the positive definiteness of their LHS matrices. Hence, as shown before, the TD-DP-FETI has been able to retain this desirable property of the original FETD method. Another observation is that the TD-DP-FETI occupies more memory than the FETD, as it involves calculation of extra matrices. However, it should be noted that the memory consumed by a program depends on many different factors, including programming skills. Moreover, the codes are implemented in MATLAB which has many limitations. Therefore, the numbers reported in the table do not show the true memory that the FETD and TD-DP-FETI really need. Finally, it can be also observed that the TD-DP-FETI converges in only 78 CG iterations while the FETD requires more than 1100 iterations. This is a consequence of the improved condition number of the TD-DP-FETI compared

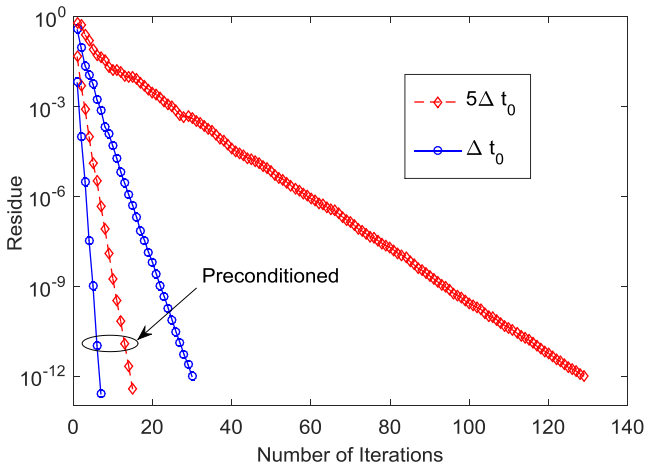

Fig. 11. The convergence history of the CG method pertaining to the global interface problem of the 16×28 EBG structure at $t = 1350\Delta t_0$ for two different time steps.

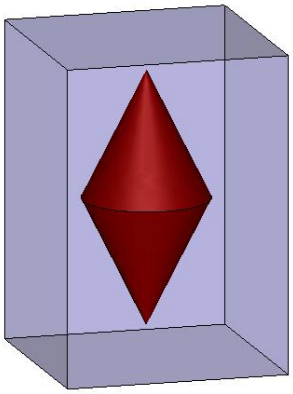

Fig. 12. A dielectric double-cone is placed in the center of a unit cell.

to the FETD. Fast convergence of the TD-DP-FETI leads to a shorter simulation time. The required time to complete one time-step is reduced by around 50%. It should be emphasized that a distinguishing feature of the FETI is its strong amenability to parallel computing. In [12], the parallel efficiency of a TD-FETI is carefully studied. It is shown that the parallel FETD performs even better than the parallel TD-FETI when implemented on small number of processors. However, as the number of processors is increased, the performance of the TD-FETI algorithm increases dramatically. Due to the similarities between the TD-FETI in [12] and the proposed TD-DP-FETI, a similar behaviour is expected. The speedup reported in Table II is because of parallel computation of matrix-vector operations by MATLAB, which does not reveal the true power of parallel TD-DP-FETI. Finally, increasing the time-step size leads to a similar increase in the CG iteration count of the FETD and TD-DP-FETI; hence, they are not reported here.

V. Conclusion and Future Work

The paper has presented a TD-DP-FETI domain decomposition method to efficiently solve large-scale transient electromagnetic problems. The method can be considered as an extension of the DP-FETI with a Dirichlet-type transmission condition to the time domain in which the continuity of $\{\dot{e}\}$ is enforced, instead of $\{e\}$, across the interfaces. It has been proven that this guarantees unconditional stability and preserves the total discrete electromagnetic energy stored in the problem during time-marching. The improved condition number of the global interface problem compared to the standard FETD results in a faster converges of the iterative solver. The formulation is especially suitable for parallel computing through which a remarkable speedup can be gained. In particular, the subdomain problems are independent and, thus, embarrassingly parallelizable. Efficient parallel implementation of the method on many-core architectures is an interesting avenue for future work.

Four numerical examples were considered to show correctness and efficiency of the method. The first two were mainly designed to study accuracy and fundamental properties of the method. Their numerical results have matched perfectly the reference solutions and confirmed stability and energy conservation of the method. The last two examples have shown that the proposed TD-DP-FETI retains numerical scalability properties of the standard FETD. This is due to the fact that both of these formulations have symmetric and PD LHS matrices. However, the TD-DP-FETD converges much faster.

In order to increase the accuracy, higher order basis functions can be employed. Moreover, the first order ABC implemented here can be easily replaced with more accurate ABCs without changing the overall framework of the formulation. An example of combining [8] with a second-order ABC is given in [34].

This formulation is so flexible, in its ultimate form, that not only does it allow using different time-step sizes in each subdomain (known as multi-time-step or subcycling) but also its stability condition can be independently adjusted in each subdomain through the variable β [20]. This is a very important property, as, depending on the mesh size and material properties in each subdomain, the time-step size determined by the stability condition may vary significantly from one subdomain to another and choosing one single time-step for the whole problem can considerably slow down the simulation (see [16], [23] for more in-depth discussions). Sometimes this restriction is so harsh that the user may prefer to use an unconditionally stable scheme (i.e. setting β to $1/4$ just like the proposed method), at least, in some subdomains. This paper has focused on the synchronous case (a unified Δt for all subdomains) and assumed $\beta = 1/4$ everywhere. Future work will investigate applications of multi-time-step, multi-β, and non-matching grids techniques to the TD-DP-FETI in electromagnetics.

It should be noted that the scalability of the proposed method is only investigated by 2-D extended arrays. It may deteriorate for 3-D extended arrays with lossless materials, as it is the case for frequency-domain DP-FETIs. However, we believe that deterioration would be slight in the TD-DP-FETI because $[\mathcal{R}_\lambda]$ is proven to remain PD under any condition.

As a final note, there exist some other preconditioning techniques introduced for the DP-FETI—see [3], [35] and the references cited therein. They may not converge as quickly as the Dirichlet preconditioner in terms of the number of itera-

TABLE II
COMPUTATIONAL STATISTICS OF THE FETD AND TD-DP-FETI METHODS FOR VARIOUS DOUBLE-CONE ARRAY SIMULATIONS.

	Method	Array size		
		10×10	20×20	30×30
Average number of CG iterations	FETD	1102	1103	1103
	TD-DP-FETI	78	78	78
Average elapsed time per time-step (s)	FETD	98.03	396.06	962.32
	TD-DP-FETI	51.46	203.43	486.09
Memory used (MB)	FETD	448	969	1,836
	TD-DP-FETI	1,094	2,268	4,309
Total number of unknowns		1,478,300	5,913,200	13,304,700
Total number of dual unknowns		111,690	470,820	1,077,350
Total number of corner unknowns		810	3,610	8,410

tions; however, they may decrease total cost of a simulation with a moderate increase in the iteration count.

ACKNOWLEDGMENT

The financial support of the Iran's National Elite Foundation through the Chamran postdoctoral fellowship award is gratefully acknowledged.

REFERENCES

[1] C. Farhat and F. Roux, "A method of finite element tearing and interconnecting and its parallel solution algorithm," *Int. J. Numer. Methods Eng.*, vol. 32, no. 6, pp. 1205–1227, Oct. 1991.

[2] C. Farhat *et al.*, "FETI-DP: a dual-primal unified FETI method-part I: a faster alternative to the two-level FETI method," *Int. J. Numer. Methods Eng.*, vol. 50, pp. 1523–1544, Mar. 2001.

[3] ——, "FETI-DPH: a dual-primal domain decomposition method for acoustic scattering," *J. Comput. Acoust.*, vol. 13, pp. 499–524, Sep. 2005.

[4] C. T. Wolfe, U. Navsariwala, and S. D. Gedney, "A parallel finite-element tearing and interconnecting algorithm for solution of the vector wave equation with PML absorbing medium," *IEEE Trans. Antennas Propag.*, vol. 48, no. 2, pp. 278–284, Feb. 2000.

[5] S.-C. Lee, M. N. Vouvakis, and J.-F. Lee, "A non-overlapping domain decomposition method with non-matching grids for modeling large finite antenna arrays," *J. Comput. Phys.*, vol. 203, pp. 1–21, Feb. 2005.

[6] M. N. Vouvakis, Z. Cendes, and J.-F. Lee, "A FEM domain decomposition method for photonic and electromagnetic band gap structures," *IEEE Trans. Antennas Propag.*, vol. 54, no. 2, pp. 721–733, Feb. 2006.

[7] Y. Li and J.-M. Jin, "A vector dual-primal finite element tearing and interconnecting method for solving 3-D large-scale electromagnetic problems," *IEEE Trans. Antennas Propag.*, vol. 54, no. 10, pp. 3000–3009, Oct. 2006.

[8] Y.-J. Li and J.-M. Jin, "A new dual-primal domain decomposition approach for finite element simulation of 3-D large-scale electromagnetic problems," *IEEE Trans. Antennas Propag.*, vol. 55, no. 10, pp. 2803–2810, Oct. 2007.

[9] M.-F. Xue and J.-M. Jin, "Nonconformal FETI-DP methods for large-scale electromagnetic simulation," *IEEE Trans. Antennas Propag.*, vol. 60, no. 9, pp. 4291–4305, Sep. 2012.

[10] C. Farhat, L. Crivelli, and F. Roux, "A transient FETI methodology for large-scale parallel implicit computations in structural mechanics," *Int. J. Numer. Methods Eng.*, vol. 37, no. 11, pp. 1945–1975, Oct. 1994.

[11] C. Farhat, P.-S. Chen, and J. Mandel, "A scalable Lagrange multiplier based domain decomposition method for time-dependent problems," *Int. J. Numer. Methods Eng.*, vol. 38, pp. 3831–3853, 1995.

[12] U. D. Navsariwala and S. D. Gedney, "An efficient implementation of the finite-element time-domain algorithm on parallel computers using a finite-element tearing and interconnecting algorithm," *Microw. Opt. Technol. Lett.*, vol. 16, no. 4, pp. 204–208, Nov. 1997.

[13] T. Lu and J.-M. Jin, "Transient electrical-thermal analysis of 3-D power distribution network with FETI-enabled parallel computing," *IEEE Trans. Compon., Packag., Manuf. Technol.*, vol. 4, no. 10, pp. 1684–1695, Oct. 2014.

[14] ——, "Coupled electrical-thermal-mechanical simulation for the reliability analysis of large-scale 3-D interconnects," *IEEE Trans. Compon., Packag., Manuf. Technol.*, vol. 7, no. 2, pp. 229–237, Feb. 2017.

[15] W. Daniel, "The subcycled Newmark algorithm," *Comput. Mech.*, vol. 20, pp. 272–281, 1997.

[16] A. Gravouil and A. Combescure, "Multi-time-step explicit-implicit method for non-linear structural dynamics," *Int. J. Numer. Methods Eng.*, vol. 50, no. 1, pp. 199–225, Jan. 2001.

[17] A. Prakash and K. D. Hjelmstad, "A FETI-based multi-time-step coupling method for Newmark schemes in structural dynamics," *Int. J. Numer. Methods Eng.*, vol. 61, pp. 2183–2204, 2004.

[18] O. S. Bursi *et al.*, "Novel generalized-α methods for interfield parallel integration of heterogeneous structural dynamics systems," *J. Comput. Appl. Math.*, vol. 234, no. 7, pp. 2250–2258, Aug. 2010.

[19] N. Mahjoubi *et al.*, "A monolithic energy conserving method to couple heterogeneous time integrators with incompatible time steps in structural dynamics," *Comput. Methods Appl. Mech. Eng.*, vol. 200, pp. 1069–1086, 2011.

[20] S. Karimi and K. B. Nakshatrala, "On multi-time-step monolithic coupling algorithms for elastodynamics," *J. Comput. Phys.*, vol. 273, pp. 671–705, 2014.

[21] W. Subber and K. Matouš, "Asynchronous space-time algorithm based on a domain decomposition method for structural dynamics problems on non-matching meshes," *Comput. Mech.*, vol. 57, pp. 211–235, 2016.

[22] A. Akbarzadeh-Sharbaf and D. D. Giannacopoulos, "On the development of nonoverlapping and stable hybrid FETD-FDTD formulations," *IEEE Trans. Antennas Propag.*, vol. 62, no. 12, pp. 6299–6306, Dec. 2014.

[23] H. Moon *et al.*, "Trade-offs for unconditional stability in the finite-element time-domain method," *IEEE Microw. Wireless Compon. Lett.*, vol. 24, no. 6, pp. 361–363, Jun. 2014.

[24] M. Géradin and D. Rixen, *Mechanical Vibrations: Theory and Applications to Structural Dynamics*, 2nd ed. Chichester, UK: John Wiley & Sons Ltd., 1997.

[25] M. Géradin and A. Cardona, *Flexible Multibody Dynamics: A Finite Element Approach*. Chichester, UK: John Wiley & Sons Ltd., 2001.

[26] J.-M. Jin, *The Finite Element Method in Electromagnetics*, 3rd ed. New York: Wiley, 2014.

[27] N. Newmark, "A method of computation for structural dynamics," *J. Eng. Mechanics Division*, vol. 85, pp. 67–94, Jul. 1959.

[28] G. H. Golub and C. F. Van Loan, *Matrix Computations*, 4th ed. Johns Hopkins University Press, 2012.

[29] D. Rixen and C. Farhat, "A simple and efficient extension of a class of substructure based preconditioners to heterogeneous structural mechanics problems," *Int. J. Numer. Methods Eng.*, vol. 44, pp. 489–516, Feb. 1999.

[30] B. Straughan, *The Energy Method, Stability, and Nonlinear Convection*, 2nd ed. New York: Springer, 2004.

[31] U. Ayachit, *The ParaView Guide: A Parallel Visualization Application*. Kitware, 2015.

[32] Z. Lou and J.-M. Jin, "A dual-field domain-decomposition method for the time-domain finite-element analysis of large finite arrays," *J. Comput. Phys.*, vol. 222, pp. 408–427, 2007.

[33] A. Barka and F.-X. Roux, "Validation of FETI-2LM formulation for EBG material prediction and optimal strategy for multiple RHS (invited)," in *2013 Proceedings of the International Symposium on Antennas Propagation*, vol. 01, Oct. 2013, pp. 80–83.

[34] Y.-J. Li and J.-M. Jin, "Implementation of the second-order ABC in the FETI-DPEM method for 3D EM problems," *IEEE Trans. Antennas Propag.*, vol. 56, no. 8, pp. 2765–2769, Aug. 2008.

[35] M.-F. Xue and J.-M. Jin, "A preconditioned dual-primal finite element tearing and interconnecting method for solving three-dimensional time-harmonic Maxwell's equations," *J. Comput. Phys.*, vol. 274, pp. 920–935, 2014.

Ali Akbarzadeh-Sharbaf received the Ph.D. degree in electrical engineering from McGill University, Montréal, Canada in 2016.

His research interests include computational electromagnetics, especially transient differential-based techniques.

Vahid Mohtashami received the B.Sc. degree (with highest distinction) in electrical engineering from Ferdowsi University of Mashhad, Iran, in 2006 and the M.Sc. and Ph.D. degrees in electrical engineering from Sharif University of Technology, Iran in 2008 and 2013 respectively. Since 2013, he has joined the Electrical Engineering Department of Ferdowsi University of Mashhad as an assistant professor. His research interests include wave propagation modelling, high-frequency scattering and numerical electromagnetics.

Dennis D. Giannacopoulos received the B.Eng. ('92) and Ph.D. ('99) degrees in electrical engineering from McGill University, Montréal, Canada. He has been with the Department of Electrical and Computer Engineering at McGill University since 2000, where he is currently an Associate Professor and a member of the Computational Electromagnetics Group. He was the recipient of the Faculty of Engineering's Samuel & Ida Fromson Award of Outstanding Teaching in 2016 and his department's Professor of the Year Award twice. His research interests include adaptive finite element analysis for electromagnetics and the acceleration of computational electromagnetics algorithms on emerging parallel architectures. He has authored or coauthored more than 125 referred journal and conference publications. His students have received several best paper or presentation awards at international conferences and symposia. His research has been sponsored by the Natural Sciences and Engineering Research Council of Canada (NSERC), the Fonds de recherche du Québec - Nature et technologies (FQRNT), and the Canada Foundation for Innovation (CFI). He has served on the editorial boards and technical program committees of several major international conferences and served as Co-Chair of the editorial board for the 14th and the 20th Conferences on the Computation of Electromagnetic Fields. He is a member of the IEEE, the International Compumag Society, and the Ordre des Ingeniuers du Québec.